
Optimal Transport on the Manifold of SPD Matrices for Domain Adaptation

Or Yair¹ Felix Dietrich² Ronen Talmon¹ Ioannis G. Kevrekidis³

Abstract

In this paper, we address the problem of Domain Adaptation (DA) using Optimal Transport (OT) on Riemannian manifolds. We model the difference between the two domains by a diffeomorphism and use the polar factorization theorem to claim that OT is indeed optimal for DA in a well-defined sense, up to a volume preserving map. We then focus on the manifold of Symmetric and Positive-Definite (SPD) matrices, whose structure provided a useful context in recent applications. We demonstrate the polar factorization theorem on this manifold. Due to the uniqueness of the weighted Riemannian mean, and by exploiting existing regularized OT algorithms, we formulate a simple algorithm that maps the source domain to the target domain. We test our algorithm on two Brain-Computer Interface (BCI) data sets and observe state of the art performance.

1. Introduction

In many applications, the acquired data sets do not reside in the same domain. Many factors can contribute to this problem; below we outline just a few notable examples that often are encountered in applications involving measured data. (i) Acquisition systems and equipment: different sets are obtained by similar but not identical sensors, possibly stemming from different calibrations. (ii) Settings and configurations: when measuring physiological signals, environmental parameters such as the room temperature or the time of day affect the recorded signals. (iii) Different sites and subjects: in the BCI tasks we consider in the present work, different data sets are recorded from different subjects performing similar tasks. DA methods are developed for alleviating the differences between the data sets stemming from such factors (Daume III & Marcu, 2006; Gong et al., 2012).

¹Viterbi Faculty of Electrical Engineering, Technion, Israel Institute of Technology ²Technical University of Munich ³Department of Chemical and Biomolecular Engineering, Johns Hopkins University. Correspondence to: Or Yair <oryair@campus.technion.ac.il>.

To make the problem and setting more concrete, consider classification tasks, which typically involve two sets: a training set and a test set. We remark that in the context of the present work, we refer to the two sets as a source set and a target set, respectively. Ideally, the two sets should be similar, but, due to various factors such as the ones mentioned above, they are in fact significantly different. This often leads to poor generalization between the sets despite their informative common internal structure, calling for DA solutions to mitigate the discrepancy between the training (source) and test (target) sets.

Here, we focus on the problem of DA on the cone manifold of SPD matrices. This particular interest arises because SPD matrices have proven to be useful features in many machine learning tasks; see for example Pennec et al. (2006); Arsigny et al. (2007); Wang et al. (2012); Jayasumana et al. (2013); Barachant et al. (2013) and references therein. In addition, SPD matrices represent a broad family; while the use of SPD *covariance* matrices is perhaps the most prominent and widely-spread, there exist other important types of SPD matrices for data analysis such as kernel matrices, diffusion tensor images, graph-related operators, and many more (Wang et al., 2015). Naturally, the problem of DA carries over from the data to their (SPD) features (Freifeld et al., 2014).

In this paper, we follow a recent line of work (see for example Courty et al. (2017) and references therein) and propose to solve an OT problem in order to obtain a transportation plan which matches between the source data distribution and the target data distribution. While the vast majority of methods solve and implement OT in Euclidean space, in this work we propose to consider OT on the cone manifold of SPD matrices. Due to the properties of the SPD cone manifold, the transportation plan induces a unique mapping between the two sets, which in turn prescribes an easy-to-implement algorithm for DA on the SPD cone manifold. This method can be carried out in a purely unsupervised manner, where the observed sets are label free. In the supervised case, where the observed sets are associated with labels, we incorporate appropriate regularization terms, which exploit the knowledge of the labels (in the training set) as presented by Courty et al. (2014). Importantly, the proposed method can be applied in a similar manner to other manifolds such as the Grassmannian manifold or the Stiefel

manifold, which are also useful for high-dimensional data representation.

The analysis of the proposed approach is based on the polar factorization theorem, which provides an informative view on the usage of OT for DA. Particularly, we show that the polar factorization theorem implies that OT is indeed optimal for DA in a well-defined sense: it can recover the correct transformation up to a volume preserving map. This result highlights the advantages of this approach, but also, and perhaps more importantly, it establishes a fundamental limitation that applies to every DA method in an unsupervised setting that takes into account only the data densities. We illustrate the theoretical results on toy examples and show state of the art numerical results on two BCI data sets.

In summary, our main contributions are as follows. (i) Based on the polar factorization theorem for diffeomorphisms on Riemannian manifolds, we present a new analysis, highlighting the advantages and limitations of OT for DA. Our analysis includes the general Riemannian setting with the particular SPD manifold as a special case. (ii) We propose a well-defined and easy to implement algorithm for DA with OT on the manifold of SPD matrices. (iii) We show that the applications of the proposed algorithm to two BCI data sets achieve state of the art results.

2. Preliminaries

2.1. The Cone Manifold of SPD Matrices

We give a brief overview of the Riemannian geometry of the cone manifold of SPD matrices. For more details, we refer the reader to Bhatia (2009). A real symmetric matrix $\mathbf{P} \in \mathbb{R}^{d \times d}$ is positive-definite if and only if it has only strictly positive eigenvalues. The collection of all SPD matrices constitutes a convex half-cone in the vector space of real $d \times d$ symmetric matrices. This cone forms a differentiable Riemannian manifold \mathcal{P}_d equipped with the following inner product at the tangent space $\mathcal{T}_{\mathbf{P}}\mathcal{P}_d$ (the space of symmetric matrices) at the point $\mathbf{P} \in \mathcal{P}_d$

$$\langle \mathbf{A}, \mathbf{B} \rangle_{\mathcal{T}_{\mathbf{P}}\mathcal{P}_d} = \langle \mathbf{P}^{-\frac{1}{2}} \mathbf{A} \mathbf{P}^{-\frac{1}{2}}, \mathbf{P}^{-\frac{1}{2}} \mathbf{B} \mathbf{P}^{-\frac{1}{2}} \rangle, \quad (1)$$

where $\mathbf{A}, \mathbf{B} \in \mathcal{T}_{\mathbf{P}}\mathcal{P}_d$ are symmetric matrices, and $\langle \cdot, \cdot \rangle$ is the Euclidean inner product operation.

\mathcal{P}_d is a Hadamard manifold, namely, it is simply connected and a complete Riemannian manifold of non-positive sectional curvature. Manifolds with non-positive curvature have a unique geodesic between any two points. The geodesic between $\mathbf{P} \in \mathcal{P}_d$, and $\mathbf{Q} \in \mathcal{P}_d$ is given by

$$\varphi(t) = \mathbf{P}^{\frac{1}{2}} (\mathbf{P}^{-\frac{1}{2}} \mathbf{Q} \mathbf{P}^{-\frac{1}{2}})^t \mathbf{P}^{\frac{1}{2}}, \quad 0 \leq t \leq 1, \quad (2)$$

see Bhatia (2009). The arc-length of the geodesic curve defines the following Riemannian distance

$$d_R^2(\mathbf{P}, \mathbf{Q}) = \left\| \log \left(\mathbf{Q}^{-\frac{1}{2}} \mathbf{P} \mathbf{Q}^{-\frac{1}{2}} \right) \right\|_F^2, \quad \mathbf{P}, \mathbf{Q} \in \mathcal{P}_d \quad (3)$$

where, $\| \cdot \|_F$ is the Frobenius norm, and $\log(\mathbf{P})$ is the matrix logarithm. For more details on \mathcal{P}_d , please see the Supplemental Material (SM).

2.2. Optimal Transport on Riemannian Manifolds

Let (\mathcal{M}, g) be a smooth, connected, oriented, d -dimensional Riemannian manifold with metric g . Let $c(p, q)$ be the ‘‘cost of moving a unit of mass’’ from point p to point q on \mathcal{M} , and define two finite Borel measures μ_1, μ_2 that are absolutely continuous with respect to the volume form of \mathcal{M} so that they have densities f_1, f_2 . Then, the Kantorovich OT problem consists of finding a transport plan $\gamma^* : \mathcal{M} \times \mathcal{M} \rightarrow \mathbb{R}$ that solves

$$\inf_{\gamma} \int_{\mathcal{M} \times \mathcal{M}} c(p, q) d\gamma(p, q). \quad (4)$$

The infimum ranges over all plans γ with $f_2(p) = \int_{\mathcal{M}} \gamma(p, \cdot) d\text{vol}$ and $f_1(q) = \int_{\mathcal{M}} \gamma(\cdot, q) d\text{vol}$. In our case, we choose the cost function $c(p, q) = d_R^2(p, q)$, where $d_R(p, q)$ is the Riemannian distance between two points $p, q \in \mathcal{M}$ induced by g . This cost function is well-studied in the theory of OT, see Villani (2009); Fathi & Figalli (2010). In particular, the given assumptions on the measures μ_1, μ_2 result in a unique solution γ^* to (4) that is concentrated on the graph of an invertible function $t : \mathcal{M} \rightarrow \mathcal{M}$ such that $\mu_2(V) = \mu_1(t^{-1}(V))$ for all measurable sets $V \subset \mathcal{M}$.

If the densities of the two measures are sampled at N_1 and N_2 discrete points respectively, they can be represented by vectors $\hat{\mathbf{f}}_1 \in \mathbb{R}^{N_1}$, $\hat{\mathbf{f}}_2 \in \mathbb{R}^{N_2}$. This leads to the discrete version of (4):

$$\min_{\Gamma \in \mathcal{F}} \langle \Gamma, \mathbf{C} \rangle, \quad (5)$$

where $\mathcal{F} = \left\{ \Gamma \in \mathbb{R}^{N_1 \times N_2} \mid \Gamma \mathbf{1}_{N_2} = \hat{\mathbf{f}}_1, \Gamma^T \mathbf{1}_{N_1} = \hat{\mathbf{f}}_2 \right\}$. $\mathbf{C} \in \mathbb{R}^{N_1 \times N_2}$ represents the transport cost between the N_1 points in the source set and the N_2 points in the target set.

3. Optimal Transport for Domain Adaptation

3.1. Domain Adaptation – Problem Formulation

In the discrete space, as described in Section 2.2 leading to (5), we consider two settings: supervised and unsupervised. In the supervised setting, consider two sets: a source set $\{\mathbf{P}_i \in \mathcal{M}\}_{i=1}^{N_1}$ and a target set $\{\mathbf{Q}_j \in \mathcal{M}\}_{j=1}^{N_2}$ and suppose the two sets are associated with labels $y_i \in \mathcal{Y}$, such that $\mathcal{P} = \{(\mathbf{P}_i, y_i)\}$ and $\mathcal{Q} = \{(\mathbf{Q}_j, y_j)\}$, where \mathcal{Y} is the set of all possible labels. The two sets reside in the same space \mathcal{M} but

are sampled from different densities with possibly different supports. As a result, the two sets can be concentrated in different parts of the space \mathcal{M} , and hence, viewed as if they live in different domains.

The source set \mathcal{P} is treated as the training set, hence, we have access to its labels, whereas the target set \mathcal{Q} is treated as the test set, and therefore its labels are considered unknown. Since the source set and the target set do not live in the same domain, the source set might not be a “good” training set for the target (test) set. The goal in DA is to find a function $s : \mathcal{M} \rightarrow \mathcal{M}$, which maps the source set from the source domain to the target domain, that is $\tilde{\mathcal{P}} = s(\mathcal{P})$, such that (i) $\tilde{\mathcal{P}}$ resides in the target domain, i.e., has a similar distribution as \mathcal{Q} , (ii) $\tilde{\mathcal{P}}$ maintains the distribution of labels of \mathcal{P} , i.e., nearby samples with similar labels in \mathcal{P} remain nearby in $\tilde{\mathcal{P}}$, and (iii) $\tilde{\mathcal{P}}$ has a meaningful similarity to \mathcal{Q} , that is we can measure the quality of s by the accuracy of a classifier trained on $\tilde{\mathcal{P}}$ and tested on \mathcal{Q} .

In unsupervised setting, we have two unlabeled sets $\mathcal{P} = \{\mathbf{P}_i\}_{i=1}^{N_1}$ and $\mathcal{Q} = \{\mathbf{Q}_i\}_{i=1}^{N_2}$. Then, DA is similarly defined, where the properties (ii) and (iii) above are redefined according to the specific task at hand, e.g., by replacing the access to labels with statistical features.

We remark that in a continuous setting, as described in Section 2.2 leading to (4), we replace the two sets \mathcal{P} and \mathcal{Q} with the two measures μ_1 and μ_2 . Assume the measure μ_2 is related to μ_1 through a diffeomorphism $s : \mathcal{M} \rightarrow \mathcal{M}$ such that for all measurable subsets $V \subset \mathcal{M}$, we have

$$\mu_2(V) = \mu_1(s^{-1}(V)). \quad (6)$$

In the context of DA, the map s represents the discrepancy between the source domain and the target domain, which we try to bridge. With these prerequisites, we ask: *given only μ_1 and μ_2 (or their densities f_1 and f_2 , respectively), how much of the information in s can be recovered?*

3.2. The Polar Factorization Theorem

McCann (2001) proved a theorem stating that diffeomorphisms s on Riemannian manifolds have a polar factorization

$$s = t \circ u, \quad (7)$$

where t is the solution to an OT problem between the two measures μ_1 and μ_2 that are related by (6), and $u : \mathcal{M} \rightarrow \mathcal{M}$ is a volume-preserving map such that $\mu_1 = \mu_1 \circ u^{-1}$. The decomposition (7) is unique, because the OT problem has a unique solution t , and thus $u = t^{-1} \circ s$ is also unique (uniqueness is defined up to sets of measure zero, see McCann (2001) for compact manifolds and Fathi & Figalli (2010) for noncompact manifolds). It can further be shown that t is the solution to OT if and only if it can be expressed as the gradient of a function ψ that is c -convex with respect

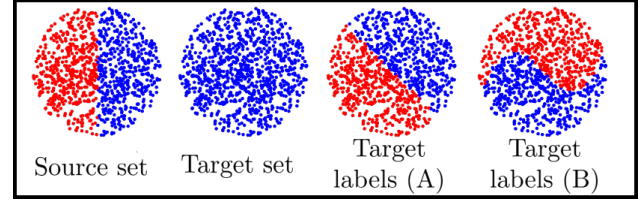


Figure 1. Consider the above (labeled) source set and (unlabeled) target set. Due to rotational symmetries, recovering the true map s (leading to either target labels A or B) by applying OT based only on the target density is impossible. McCann’s polar factorization theorem implies that this limitation is fundamental and applies in general to DA in unsupervised settings.

to the cost function c (see Brenier (1991); McCann (2001); Modin (2017)).

The polar factorization (7) enables us to present a new analysis for DA using OT. Broadly, McCann’s theorem implies that in an unsupervised setting, when we only have access to the densities, the map $s = t \circ u$, which represents the difference between the source and target domains, can be recovered up to a volume preserving function by employing OT. This fundamental limitation is *common to all methods relying on empirical densities* for unsupervised domain adaptation as illustrated in Figure 1. More specifically, if for a given map s , the map u in (7) is the identity, solving the OT problem recovers the map s . However, if u is not the identity map, solving the OT problem will only recover a function $t \circ \tilde{u}$ for some volume preserving \tilde{u} . This means that the correct target density will be recovered, but the approach may still fail to provide the correct point-wise mapping s between the source and the target domains, and hence fail to provide the correct labels on the target domain. The further the map u is away from the identity map, the more distortion is introduced into the adaptation. If the map u is known, such a “distance” from the identity map can be measured, for example, in the L^2 -norm on the space of smooth functions $C^\infty(\mathcal{M})$ on the manifold.

3.3. Domain Adaptation in a Euclidean Space

When $\mathcal{M} = \mathbb{R}^d$ equipped with the standard Euclidean 2-norm, and if the map s is linear, McCann’s polar factorization theorem reduces to polar decomposition of matrices (see Brenier (1991)), namely:

$$s(\mathbf{x}) = \mathbf{S}\mathbf{x} = \mathbf{T}\mathbf{U}\mathbf{x} \quad (8)$$

where $\mathbf{x} \in \mathbb{R}^d$, $\mathbf{S} \in \mathbb{R}^{d \times d}$ is invertible, $\mathbf{T} = (\mathbf{S}\mathbf{S}^T)^{\frac{1}{2}} > 0$, and $\mathbf{U} = \mathbf{T}^{-1}\mathbf{S}$ is orthogonal.

An analogous result to the celebrated result of Brenier on the unit sphere (Brenier, 1987; 1991) was proven in Courty et al. (2017):

Theorem 1 (Discrete case (Courty et al., 2017)) Let μ_1 and μ_2 be two discrete distributions with N Diracs. If the following conditions hold. (i) The source sample in $\mathbf{x}_i \in \mathbb{R}^d$, $\forall i \in \{1, 2, \dots, N\}$ such that $\mathbf{x}_i \neq \mathbf{x}_j$ if $i \neq j$. (ii) All weights in the source and target distributions are $\frac{1}{N}$. (iii) The target samples are defined as $\mathbf{z}_i = \mathbf{T}\mathbf{x}_i + \mathbf{b}$, where $\mathbf{T} > 0$ (iv) The cost function is $c(\mathbf{x}, \mathbf{z}) = \|\mathbf{x} - \mathbf{z}\|_2^2$ then, the solution γ of the OT problem satisfies $\gamma(\mathbf{x}_i) = \mathbf{T}\mathbf{x}_i + \mathbf{b} = \mathbf{z}_i, \forall i \in \{1, 2, \dots, N\}$.

In short, the map $t(\mathbf{x}) = \mathbf{T}\mathbf{x} + \mathbf{b}$ (where $\mathbf{T} > 0$) is the solution to an OT problem between an atomic measure μ_1 and $\mu_2 = \mu_1 \circ t^{-1}$. Using the polar factorization theorem in the Euclidean case described above, we can provide an elegant new proof to the continuous counterpart of Theorem 1 in the continuous case.

Theorem 2 (Continuous case) The map $t(\mathbf{x}) = \mathbf{T}\mathbf{x} + \mathbf{b}$ (where $\mathbf{T} > 0$) is the solution to an OT problem between a measure μ_1 and a measure $\mu_2 = \mu_1 \circ t^{-1}$ with the cost $c(\mathbf{x}, \mathbf{z}) = \|\mathbf{x} - \mathbf{z}\|_2^2$.

Proof 1 Consider the function $\psi(\mathbf{x}) = \frac{1}{2}\mathbf{x}^T\mathbf{T}\mathbf{x} + \mathbf{b}^T\mathbf{x}$. Since $\mathbf{T} > 0$, ψ is c -convex with respect to the cost $c(\mathbf{x}, \mathbf{z}) = \|\mathbf{x} - \mathbf{z}\|_2^2$. In addition, $\nabla\psi = t$, and therefore, by the polar factorization theorem, the map $t(\mathbf{x}) = \mathbf{T}\mathbf{x} + \mathbf{b}$ is the solution to the OT problem.

In this work we focus on the cone manifold of SPD matrices \mathcal{P}_d . Consider the following linear map on \mathcal{P}_d , with a fixed, real-valued, invertible matrix \mathbf{S} :

$$s(\mathbf{P}) = \mathbf{S}\mathbf{P}\mathbf{S}^T. \quad (9)$$

Using the polar decomposition $\mathbf{S} = \mathbf{T}\mathbf{U}$, we can write $s(\mathbf{P}) = \mathbf{T}\mathbf{U}\mathbf{P}\mathbf{U}^T\mathbf{T}$. We now show an analogous proposition to Theorem 2 for the the SPD case (with Euclidean cost function).

Corollary 1 (SPD case with square Euclidean cost) The linear map $\mathbf{Q} = t(\mathbf{P}) = \mathbf{T}\mathbf{P}\mathbf{T}$ (where $\mathbf{T} > 0$) is the solution to an OT problem between μ_1 and $\mu_2 = \mu_1 \circ t^{-1}$ on \mathcal{P}_d with $c(\mathbf{P}, \mathbf{Q}) = \|\mathbf{P} - \mathbf{Q}\|_F^2$ where $\mathbf{P}, \mathbf{Q} \in \mathcal{P}_d$.

Proof 2 Using the $\text{vec}(\cdot)$ operator we can write $\mathbf{q} = (\mathbf{T} \otimes \mathbf{T})\mathbf{p}$, where $\mathbf{q} = \text{vec}(\mathbf{Q})$, $\mathbf{p} = \text{vec}(\mathbf{P})$, and \otimes is the Kronecker product. Since $\mathbf{T} > 0$, then $(\mathbf{T} \otimes \mathbf{T}) > 0$ as well. Therefore, by Theorem 2, $t(\mathbf{p}) = (\mathbf{T} \otimes \mathbf{T})\mathbf{p}$ is the solution to the OT problem between μ_1 and $\mu_2 = \mu_1 \circ t^{-1}$ with the given cost function.

We conjecture that in this linear case the map t is the solution to the OT problem on \mathcal{P}_d with $c(\mathbf{P}, \mathbf{Q}) = d_R^2(\mathbf{P}, \mathbf{Q})$ as well, i.e., with the cost defined through the Riemannian distance. We leave the proof for future work, yet, in the following, we present empirical evidence supporting this

conjecture. More importantly, in the general case, the OT plan obtained using the Euclidean distance could be substantially different from the OT plan obtained using the Riemannian distance d_R . We postulate that the Riemannian distance d_R is the one that should be used, as it demonstrates superior results in Section 4.

3.4. Algorithm

The proposed algorithm for DA on \mathcal{P}_d appears in Algorithm 1. The algorithm maps a source set $\{\mathbf{P}_i\}_{i=1}^{N_1}$ to the domain of a target set $\{\mathbf{Q}_i\}_{i=1}^{N_2}$ and is comprised of three main steps: (i) computing histograms, (ii) solving OT, and (iii) applying the transport plan.

In the remainder of this section, we outline several implementation remarks. First, computing the histograms using uniform bins, namely, $\mathbf{p}[i] = 1/N_1$, and $\mathbf{q}[j] = 1/N_2$ for $i \in \{1, 2, \dots, N_1\}$ and $j \in \{1, 2, \dots, N_2\}$, is common practice. Yet, for real data sets of empirical observations, using Kernel Density Estimation (KDE) methods may assign weights smaller than $1/N$ to outliers far away from the true target points. These smaller weights conveniently attenuate the unwanted transport effect caused by these erroneous points, leading to a more robust algorithm. Concretely, Step 1 is replaced by $\mathbf{p}[i] = \frac{1}{Z} \sum_{j=1}^{N_1} \exp\left(-\frac{d_R^2(\mathbf{P}_i, \mathbf{P}_j)}{2\sigma^2}\right)$, where $Z \in \mathbb{R}$ is set such that $\sum_{i=1}^{N_1} \mathbf{p}[i] = 1$ and σ^2 is usually set around the median of $\{d_R^2(\mathbf{P}_i, \mathbf{P}_j)\}_{i,j}$. Step 2 for the histogram \mathbf{q} is modified in an analogous fashion.

Second, we propose to obtain the transport plan $\mathbf{\Gamma}$ in the unsupervised setting, by using the Sinkhorn OT algorithm presented by Cuturi (2013), which extends (5) and solve:

$$\min_{\mathbf{\Gamma} \in \mathcal{F}} \langle \mathbf{\Gamma}, \mathbf{C} \rangle - \frac{1}{\lambda} h(\mathbf{\Gamma}) \quad (10)$$

where $h(\mathbf{\Gamma}) = -\sum_{i=1}^{N_1} \sum_{j=1}^{N_2} \mathbf{\Gamma}[i, j] \log(\mathbf{\Gamma}[i, j])$ is the entropy of $\mathbf{\Gamma}$. See the SM for implementation details.

In the supervised setting, where the points in the source set are equipped with corresponding labels $y_i \in \mathcal{Y}$, $\{(\mathbf{P}_i, y_i)\}_{i=1}^{N_1}$, Step 4 can be replaced with a regularized version of the (Sinkhorn) optional transport proposed by Courty et al. (2014):

$$\min_{\mathbf{\Gamma} \in \mathcal{F}} \langle \mathbf{\Gamma}, \mathbf{C} \rangle - \frac{1}{\lambda} h(\mathbf{\Gamma}) + \eta \sum_{j=1}^{N_2} \sum_{y=1}^{|\mathcal{Y}|} \|\mathbf{\Gamma}(\mathcal{I}_y, j)\|_q^p \quad (11)$$

where \mathcal{I}_y is a set containing the indices of the source points associated with the label $y \in \mathcal{Y}$, $\mathbf{\Gamma}(\mathcal{I}_y, j)$ is a vector consisting of entries from the j th column of $\mathbf{\Gamma}$ associated with the label y (i.e., from rows \mathcal{I}_y) and $\|\cdot\|_q^p$ is the ℓ_q norm to the power of p . See the SM for more details.

The final remark concerns the implementation of Step 5. Step 4 results in the transport plan matrix $\mathbf{\Gamma} \in \mathbb{R}^{N_1 \times N_2}$. In

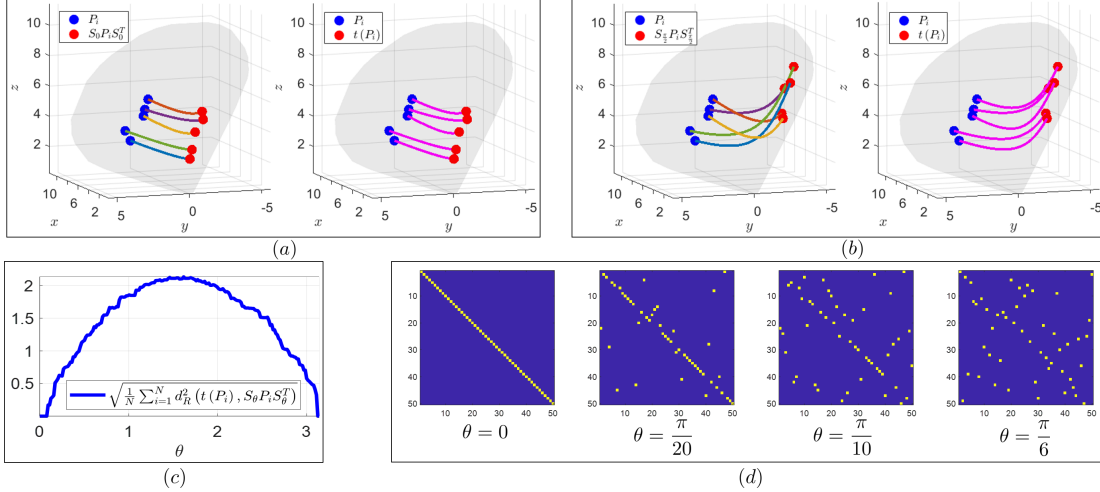


Figure 2. Results on the toy problem, please see 4.1 for details.

Courty et al. (2017) the application of the plan for DA in the Euclidean space is carried out using the map defined by the weighted mean

$$\hat{x}_i = t(x_i) = \arg \min_{x \in \mathbb{R}^n} \sum_j \Gamma[i, j] \|x - z_j\|_2^2.$$

However, when considering a general Riemannian manifold, this quantity might not be well-defined, since the Riemannian mean is not necessarily unique. Fortunately, in \mathcal{P}_d , the Riemannian weighted mean *is* unique and the optimization problem is strictly convex, see Bhatia (2009). Therefore, Step 5 consists of a well-defined map:

$$\tilde{P}_i = t(P_i) = \arg \min_{P \in \mathcal{P}_d} \sum_{j=1}^{N_2} \Gamma[i, j] d_R^2(P, Q_j) \quad (12)$$

This weighted mean problem can be solved using gradient descent based algorithms. See the SM for the implementation details. In practice, since Γ tends to be sparse, in order to reduce the computational load in Step 5 of Algorithm 1, one can use only the highest values in the i th row of Γ .

4. Experimental Results

In this section we first present two toy examples, illustrating the matrix polar decomposition and the subsequent conjecture described in Section 3.3. The second toy problem indicates a possible future direction when additional knowledge on the data is available. Then, we present results on two BCI data sets, where our method achieves state of the art performance. Our source code is available in the SM and will be publicly available upon acceptance. Additional implementation details are given in the SM.

Algorithm 1 DA using OT for SPD matrices

Input: source and target sets $\{P_i\}_{i=1}^{N_1}, \{Q_j\}_{j=1}^{N_2}$ in \mathcal{P}_d .

Output: the adapted source set $\{\tilde{P}_i\}_{i=1}^{N_1}$.

- 1: **for all** i **do:** $p[i] \leftarrow 1/N_1$. $\{i \in \{1, \dots, N_1\}\}$
- 2: **for all** j **do:** $q[j] \leftarrow 1/N_2$. $\{j \in \{1, \dots, N_2\}\}$
- 3: **for all** i and j **do:** $C[i, j] \leftarrow d_R^2(P_i, Q_j)$. $\{\text{Eq. (3)}\}$
- 4: **set:** $\Gamma \leftarrow \text{SinkhornOptimalTransport}(p, q, C)$. $\{\text{see Section 3.4}\}$
- 5: **for all** i **do:** $\{\text{see Section 3.4}\}$

$$\tilde{P}_i \leftarrow t(P_i) = \arg \min_{P \in \mathcal{P}_d} \sum_{j=1}^{N_2} \Gamma[i, j] d_R^2(P, Q_j)$$

4.1. Toy Problems

The two toy problems involve symmetric 2×2 matrices, because any symmetric 2×2 matrix $A = \begin{bmatrix} x & y \\ y & z \end{bmatrix}$ can be visualized in \mathbb{R}^3 by plotting the elements (x, y, z) . In addition, A is SPD if and only if $x, z > 0$ and $y^2 < xz$. These conditions imply that the 2×2 SPD matrices reside within a cone embedded in \mathbb{R}^3 . In both toy problems, since the problems are computationally light and the purpose of this section is to illustrate the theoretical claims regarding OT, we apply Algorithm 1 with uniform histograms and we solve the OT problem directly (5), without the Sinkhorn regularization.

Consider a 2×2 SPD matrix P and a parametric map s_θ given by $s_\theta(P) = S_\theta P S_\theta^T$, where $S = T U_\theta$, $T = \begin{bmatrix} 0.5 & -1/4 \\ -1/4 & 1 \end{bmatrix} > 0$ and $U_\theta = \begin{bmatrix} \cos(\theta) & \sin(\theta) \\ -\sin(\theta) & \cos(\theta) \end{bmatrix}$ is orthogonal. First, we generate a source set of 5 SPD matrices $\{P_i\}_{i=1}^5$ and apply s_0 and $s_{\pi/2}$ to this set, namely $\{s_\theta(P_i)\}_{i=1}^5$ is the target set. We apply Algorithm 1 to $\{P_i\}_{i=1}^5$ and $\{s_\theta(P_i)\}_{i=1}^5$.

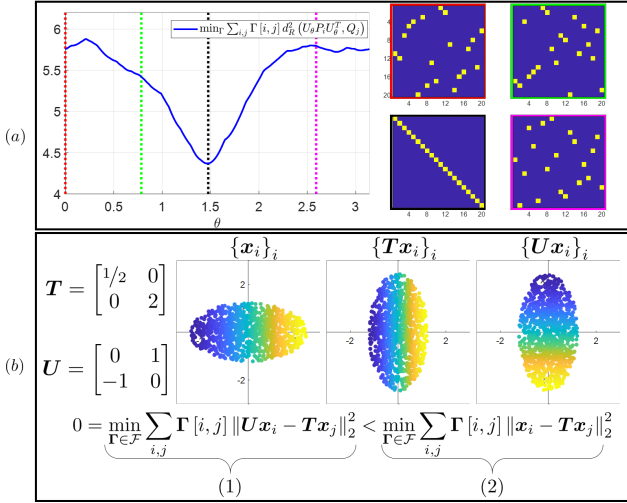


Figure 3. (a) Left – the cost function value as a function of θ . Right – the transport plan Γ for four values of θ . The red frame ($\theta = 0$) is equivalent to directly applying OT; whereas in the black frame ($\theta = \pi/2$) we first multiply the matrices P_i with $U_{\pi/2}$ and then solve the OT problem. (b) Consider the linear map $S = T$ specified above. Since $T > 0$, the theory guarantees that solving (2), will recover the true S . Solving (1) with U specified above will not recover the true S . However the value of (1) is strictly smaller than (2). A similar example can be constructed in the SPD manifold as well.

and obtain $\{t_\theta(P_i)\}_{i=1}^5$. The pairs $(P_i, s_\theta(P_i))$ embedded in \mathbb{R}^3 are depicted in Figure 2(a) and (b). In the left plots, the pairs are connected by the geodesic curves. In the right plots, the curves represent the matching obtained by t_θ computed using Algorithm 1. In Figure 2(a), where $S_0 = T > 0$ and does not contain a orthogonal component, we observe that the obtained OT t_0 indeed recovers the map s_0 . Conversely, in Figure 2(b), where $S_{\pi/2}$ has a non-trivial orthogonal component, we observe that the OT $t_{\pi/2}$ does not recover the true matching.

To quantify this observation, we generate a set of $N = 50$ SPD matrices $\{P_i\}_{i=1}^N$ and consider maps s_θ , where $\theta \in [0, \pi]$. For each value of θ , we compute t_θ using Algorithm 1. Figure 2(c) displays the error between $s_\theta(P_i)$ and the corresponding $t_\theta(P_i)$ defined by $\sqrt{\frac{1}{N} \sum_i d_R^2(t_\theta(P_i), s_\theta(P_i))}$. In addition, Figure 2(d) presents the transport plans Γ obtained for 4 values of θ . We observe that the ability of OT to recover s_θ depends on θ ; as the orthogonal component of s_θ is ‘less prominent’ (θ is closer to 0), the recovery becomes more accurate.

For some linear maps s , solving the following non-convex optimization problem:

$$\min_{U \in O} \min_{\Gamma \in \mathcal{F}} \sum_{i,j} \Gamma[i,j] d_R^2(UP_iU^T, Q_j) \quad (13)$$

where U is orthogonal, may recover the true map s . This is demonstrated on a toy problem similar to the one described above. Consider a source set $\{P_i\}_{i=1}^{N=20}$ of SPD matrices in $\mathbb{R}^{2 \times 2}$ and a target set $\{Q_i\}_{i=1}^{N=20}$, s.t. $Q_i = SP_iS^T$ for some invertible matrix S . Since in general S is not an SPD matrix, applying OT to the two sets fails to recover the correct matching. We heuristically solve (13) by: (i) sampling uniformly θ from $[0, 2\pi]$, (ii) generating the corresponding rotation matrices U_θ , and (iii) solving the inner OT problem (13), for each U_θ candidate. Note that in general, one should (exhaustively) search over a discretization of the entire space of orthogonal matrices. Figure 3(a,left) presents the cost function value as a function of θ . Figure 3(a,right) presents the transport plan Γ for four values of θ . In this example, directly applying OT to the two sets is equivalent to the result obtained for $\theta = 0$ (red frame) which does not recover the true map, whereas the min value of the (completely unsupervised) cost function (13) coincides with the true map (black frame).

Seemingly, the above experiment contradicts our main claim about the fundamental limitation of OT for DA in unsupervised setting, since the unsupervised problem (13) is shown to coincide with the true map despite having a non-trivial orthogonal part. However, even in this linear case, the fundamental limitation still holds and the minimum of the cost function does not guarantee to coincide with the correct u . Figure 3(b) provides a simple counterexample in the linear Euclidean case. Nevertheless, we believe this practice has potential when the setting is not strictly unsupervised and few source-target pairs are given. This will be further explored in future work.

4.2. Motor Imagery Task

We use data from the BCI competition IV, see Naem et al. (2006), which have been previously addressed using the Riemannian geometry of SPD matrices by Barachant et al. (2012); Zanini et al. (2018); Yair et al. (2019). The dataset contains EEG recordings from 22 electrodes from 9 subjects, where each subject was recorded in 2 different days (sessions). In repeated trials, the subjects were asked to imagine performing one out of four possible movements: (i) right hand, (ii) left hand, (iii) both feet, and (iv) tongue. Overall, in a single day, each movement was repeated 72 times by each subject. The sampling rate is 250Hz and each trial is 3 seconds long. Here, we consider only 5 subjects out of the available 9 as in Zanini et al. (2018); Yair et al. (2019). This is because the single-session single-subject classification results on data from each of the remaining 4 subjects were poor, see Ang et al. (2012); Barachant et al. (2012); Zanini et al. (2018). Thus, DA is not relevant. Let $X_i^{(k,s)} \in \mathbb{R}^{22 \times 750}$ denote the data from the i th trial of the k th subject at the s th session, and let

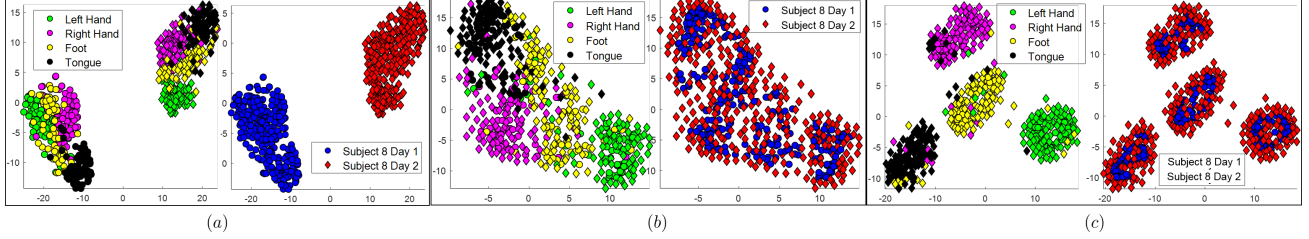


Figure 4. Cross-session adaptation in the motor imagery task. The t-SNE representation of all the SPD matrices of Subject 8: (a) before Algorithm 1, (b) after Algorithm 1 (unsupervised) and (c) after Algorithm 1 (supervised). Please see 4.2 for details.

$y_i^{(k,s)} \in \{\text{right hand, left hand, both feet, tongue}\}$ be the associated label. As in Barachant et al. (2012); Zanini et al. (2018); Yair et al. (2019), we preprocessed the data by applying a BPF with cutoff frequencies 8Hz and 30Hz. For each trial we compute the empirical covariance $\mathbf{P}_i^{(k,s)} \in \mathbb{R}^{22 \times 22}$.

To illustrate the need for DA, Figure 4(a) displays the 2-D t-SNE representation (Maaten & Hinton, 2008) of all the SPD matrices of Subject 8, namely $\{\mathbf{P}_i^{(8,s)}\}$, $i = 1, \dots, 288$, $s = 1, 2$, computed based on the pairwise Riemannian distances d_R^1 . We observe that the data is primarily clustered by session, whereas the clustering by the imagined movement is only secondary. This poses a challenge for classifiers trained on one session and applied to the other. We adapt the SPD matrices of the first session by applying Algorithm 1 twice. Once, in the unsupervised setting (without using any labels), and once, in the supervised setting (using the source labels) as described in 3.4. Let $\{\tilde{\mathbf{P}}_i^{(8,1)}\}$ denote the output of the algorithm. Figure 4(b) depicts the 2-D t-SNE representation of $\{\tilde{\mathbf{P}}_i^{(8,1)}\}$ in the unsupervised setting, and similarly, Figure 4(c) depicts the 2-D representation in the supervised setting. We observe that the data is primarily clustered by the imagined movement, whereas the session has only a mild effect. In addition, we observe the contribution of the known labels in the supervised setting. For cross-subject classification we repeat the same process, but with two different subjects instead of the same subject and two different sessions. See the SM for figures about multiple subjects adaptation.

To quantify the adaptation, we present the classification accuracy for cross-session and cross-subject classification. For the cross-subject classification, we present the average result of each subject treated as a test set for all possible cross-subject pairs (see the SM for the full detailed table). We compare the performance to three methods: (i) the method in Ang et al. (2012) which achieved the 1st place in the original competition, (ii) the Affine Transform (AT) proposed in Zanini et al. (2018), and (iii) the Parallel Transport (PT)

¹The pairwise distances d_R were used for the t-SNE representations of the covariance matrices in all other figures as well.

proposed in Yair et al. (2019). For evaluation, we use a linear SVM classifier equipped with the Euclidean approximation in the tangent space as described in the SM. Table 3(a) depicts the cross-session performance and Table 3(b) depicts the cross-subject performance. Note that the results in Ang et al. (2012) are available only for the cross-session case. In addition, in the cross-subject case, we added a variant of Algorithm 1, which relies on the Euclidean distance instead of the Riemannian distance (labeled ‘‘Euclid’’). We observe that overall Algorithm 1, with the Riemannian metric, provides the best results.

4.3. P300 Event Related Potential Task

We use data from the Brain Invaders experiment from GIPSA-lab. Here we only include a brief description; for more details see Congedo et al. (2011). In this experiment, subjects watched a screen with 36 objects flashing alternatively. Their task was to mentally count the number of flashes of the specific (a-priori known) target objects. Spotting a target generates a P300 wave, which is an Event Related Potential (ERP). Each subject watched 480 trials, of which 80 contained the target and the remaining 400 did not. The data consist of EEG recordings from 16 electrodes sampled at 512Hz. The duration of each trial is one second.

Note that the empirical covariance matrix is invariant to the temporal order of the samples, yet the ERP is a short local wave. Consequently, the covariance matrix does not capture sufficient information on the ERP in a given trial. Thus, instead of the standard covariance matrix, we use an augmented covariance matrix as proposed in Barachant & Congedo (2014). For more details on the pre-processing and the augmented covariance please see the SM. We note that, in comparison to Barachant & Congedo (2014) which used the test labels to compute the augmented covariances, we apply a completely unsupervised method. We denote the augmented covariance matrix associated with the i th trial of the k subject by $\tilde{\mathbf{P}}_i^{(k)} \in \mathbb{R}^{32 \times 32}$ (after augmenting by 16 channels the original measured 16).

To illustrate the existing batch effect in the data, and subsequently, the need for DA, Figure 5(a) displays the 2-D

Table 1. Classification accuracy in the motor imagery task. (s) stands for the supervised version, (u) stands for the unsupervised version and (E) stands for the Euclid metric.

(a) Cross session						(b) Cross subject					
Sub.	Alg.1 (s)	Alg.1 (u)	PT	AF	Ang at el.	Sub.	Alg.1 (s)	Alg.1 (u)	Alg.1 (E)	PT	AF
1	82.29	80.90	81.25	79.6	67.6	1	67.88	62.94	61.98	60.31	60.4
3	88.19	87.86	88.19	81.5	74.5	3	75.52	71.01	70.40	65.02	69.4
7	78.47	82.29	76.39	75.2	77.3	7	64.76	63.98	60.85	57.03	57.0
8	85.07	83.25	82.99	82.1	75.5	8	68.92	66.06	65.97	59.81	63.2
9	85.42	80.25	77.78	81.8	60.6	9	66.75	59.18	56.43	63.63	68.8
Mean	83.89	82.93	81.32	80	71.1	Mean	68.92	64.43	63.13	61.16	63.76

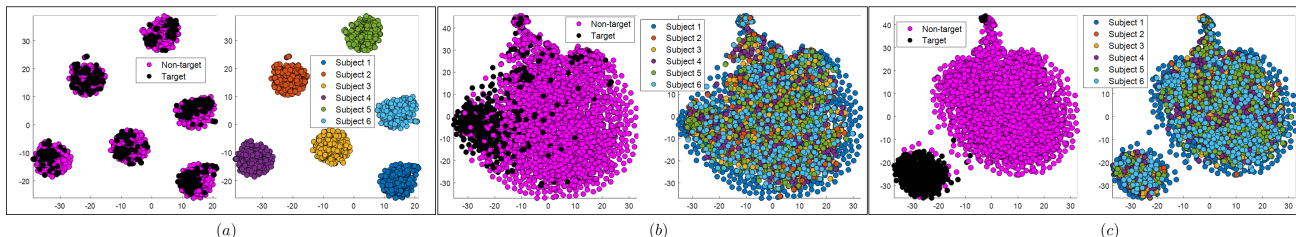


Figure 5. Cross-subject adaptation in the ERP P300 task. The t-SNE representation of the SPD matrices of three subjects: (a) before (b) after Algorithm 1 (unsupervised) and (c) after Algorithm 1 (supervised). Please see Section 4.3 for details.

t-SNE representation of the covariance matrices from all six subjects. As in the previous application, we observe that the SPD matrices are primarily clustered by the subject. Figure 5(b) displays the covariance matrices from all six subjects after applying Algorithm 1 in the unsupervised setting to adapt the SPD matrices of all subjects to the domain of the SPD matrices of Subject 1. Similarly, Figure 5(c) displays the data from all six subjects after applying Algorithm 1 in the supervised setting to adapt the SPD matrices of all subjects to the domain of the SPD matrices of Subject 1, that is, using all labels except the labels of Subject 1 (the target domain). We observe that after the adaptation the SPD matrices are clustered by label of the trial and not by subject. In addition, similarly to the previous experiment, we clearly observe the contribution of the labels in the supervised setting.

To quantify the adaptation, we computed the cross-subject classification precision, defined by $pr = \frac{TP}{TP+FP}$, where TP is the number of trials with target objects correctly classified, and FP is the number of trials without a target wrongly classified as with a target. The SM contains detailed tables of the algorithm precision performance. We compare Algorithm 1 to the algorithms presented in Zanini et al. (2018) and in Yair et al. (2019). For the comparison, we use the same Minimum Distance to Mean (MDM) classifier as in Zanini et al. (2018), which was proposed in Barachant et al. (2012). Table 2 contains a summary of the classification precision obtained by Algorithm 1 and the competing algorithms. The

Table 2. Classification precision in the ERP P300 task. (s) stands for the supervised version, (u) stands for the unsupervised version

Test sub.	Alg.1 (s)	Alg.1 (u)	PT	AT
1	91.57	88.85	93.31	86.3
2	89.71	88.68	89.55	85.8
3	96.05	95.89	91.44	N/A
4	98.07	93.99	91.45	N/A
5	96.07	94.54	90.35	86.7
6	85.44	90.00	69.17	89.6
Mean	92.87	91.99	87.55	87.1

N/A results were not reported in Zanini et al. (2018), since these subjects were classified as “bad” subjects. We observe that Algorithm 1 provides the best results overall, and that the knowledge of the labels in the supervised setting improves the classification.

5. Conclusion

In this paper we presented an approach (and the resulting algorithm) for DA on the manifold of SPD matrices using OT. Based on the polar factorization theorem, we present a new analysis, highlighting the advantages and limitations of OT for DA. Our analysis includes both the general Riemannian setting as well as the particular SPD manifold. The mapping

we derived is well-defined, and we presented an algorithm for its simple implementation. Our method achieves state of the art performance in BCI tasks.

References

- Ang, K., Chin, Z. Y., Wang, C., Guan, C., and Zhang, H. Filter bank common spatial pattern algorithm on bci competition iv datasets 2a and 2b. Frontiers in neuroscience, 6:39, 2012.
- Arsigny, V., Fillard, P., Pennec, X., and Ayache, N. Geometric means in a novel vector space structure on symmetric positive-definite matrices. SIAM journal on matrix analysis and applications, 29(1):328–347, 2007.
- Barachant, A. and Congedo, M. A plug&play P300 BCI using information geometry. arXiv preprint arXiv:1409.0107, 2014.
- Barachant, A., Bonnet, S., Congedo, M., and Jutten, C. Multiclass brain–computer interface classification by riemannian geometry. IEEE Transactions on Biomedical Engineering, 59(4):920–928, 2012.
- Barachant, A., Bonnet, S., Congedo, M., and Jutten, C. Classification of covariance matrices using a Riemannian-based kernel for bci applications. Neurocomputing, 112: 172–178, 2013.
- Bhatia, R. Positive definite matrices, volume 16. Princeton university press, 2009.
- Brenier, Y. Décomposition polaire et réarrangement monotone des champs de vecteurs. CR Acad. Sci. Paris Sér. I Math., 305:805–808, 1987.
- Brenier, Y. Polar factorization and monotone rearrangement of vector-valued functions. Communications on Pure and Applied Mathematics, 44(4):375–417, jun 1991. doi: 10.1002/cpa.3160440402.
- Congedo, M., Goyat, M., Tarrin, N., Ionescu, G., Varnet, L., Rivet, B., Phlypo, R., Jrad, N., Acquadro, M., and Jutten, C. “brain invaders”: a prototype of an open-source p300-based video game working with the openvibe platform. In 5th International Brain-Computer Interface Conference 2011 (BCI 2011), pp. 280–283, 2011.
- Courty, N., Flamary, R., and Tuia, D. Domain adaptation with regularized optimal transport. In Joint European Conference on Machine Learning and Knowledge Discovery in Databases, pp. 274–289. Springer, 2014.
- Courty, N., Flamary, R., Tuia, D., and Rakotomamonjy, A. Optimal transport for domain adaptation. IEEE transactions on pattern analysis and machine intelligence, 39(9):1853–1865, 2017.
- Cuturi, M. Sinkhorn distances: Lightspeed computation of optimal transport. In Advances in neural information processing systems, pp. 2292–2300, 2013.
- Daume III, H. and Marcu, D. Domain adaptation for statistical classifiers. Journal of artificial Intelligence research, 26:101–126, 2006.
- Fathi, A. and Figalli, A. Optimal transportation on non-compact manifolds. Israel Journal of Mathematics, 175 (1):1–59, jan 2010. doi: 10.1007/s11856-010-0001-5.
- Freifeld, O., Hauberg, S., and Black, M. J. Model transport: Towards scalable transfer learning on manifolds. In Proceedings of the IEEE Conference on Computer Vision and Pattern Recognition, pp. 1378–1385, 2014.
- Gong, B., Shi, Y., Sha, F., and Grauman, K. Geodesic flow kernel for unsupervised domain adaptation. In 2012 IEEE Conference on Computer Vision and Pattern Recognition, pp. 2066–2073. IEEE, 2012.
- Hoffmann, U., Garcia, G., Vesin, J., Diserens, K., and Ebrahimi, T. A boosting approach to p300 detection with application to brain-computer interfaces. In Conference Proceedings. 2nd International IEEE EMBS Conference on Neural Engineering, 2005., pp. 97–100. IEEE, 2005.
- Jayasumana, S., Hartley, R., Salzmann, M., Li, H., and Harandi, M. Kernel methods on the riemannian manifold of symmetric positive definite matrices. In Proceedings of the IEEE Conference on Computer Vision and Pattern Recognition, pp. 73–80, 2013.
- Maaten, L. v. d. and Hinton, G. Visualizing data using t-sne. Journal of machine learning research, 9(Nov):2579–2605, 2008.
- McCann, R. Polar factorization of maps on riemannian manifolds. Geometric & Functional Analysis GAFA, 11 (3):589–608, 2001.
- Modin, K. Geometry of matrix decompositions seen through optimal transport and information geometry. Journal of Geometric Mechanics, 9(3):335–390, jun 2017. doi: 10.3934/jgm.2017014.
- Naeem, M., Brunner, C., Leeb, R., Graimann, B., and Pfurtscheller, G. Seperability of four-class motor imagery data using independent components analysis. Journal of neural engineering, 3(3):208, 2006.
- Pennec, X., Fillard, P., and Ayache, N. A riemannian framework for tensor computing. International Journal of computer vision, 66(1):41–66, 2006.
- Tuzel, O., Porikli, F., and Meer, P. Pedestrian detection via classification on riemannian manifolds.

IEEE transactions on pattern analysis and machine intelligence, 30(10):1713–1727, 2008.

Villani, C. Optimal Transport. Springer Berlin Heidelberg, 2009. doi: 10.1007/978-3-540-71050-9.

Wang, L., Zhang, J., Zhou, L., Tang, C., and Li, W. Beyond covariance: Feature representation with nonlinear kernel matrices. In Proceedings of the IEEE International Conference on Computer Vision, pp. 4570–4578, 2015.

Wang, R., Guo, H., Davis, L. S., and Dai, Q. Covariance discriminative learning: A natural and efficient approach to image set classification. In 2012 IEEE Conference on Computer Vision and Pattern Recognition, pp. 2496–2503. IEEE, 2012.

Yair, O., Ben-Chen, M., and Talmon, R. Parallel transport on the cone manifold of spd matrices for domain adaptation. IEEE Transactions on Signal Processing, 67(7): 1797–1811, 2019.

Zanini, P., Congedo, M., Jutten, C., Said, S., and Berthoumieu, Y. Transfer learning: a riemannian geometry framework with applications to brain–computer interfaces. IEEE Transactions on Biomedical Engineering, 65(5):1107–1116, 2018.

Optimal Transport on the Manifold of SPD Matrices for Domain Adaptation – Supplementary Material

6. On the Cone Manifold of SPD Matrices – Additional Information

In this section, we provide additional information about the SPD manifold. The Exponential map from $\mathcal{T}_P\mathcal{P}_d$ to \mathcal{P}_d is given explicitly by

$$\mathbf{P}_i = \text{Exp}_P(\mathbf{A}_i) = \mathbf{P}^{\frac{1}{2}} \exp(\mathbf{P}^{-\frac{1}{2}} \mathbf{A}_i \mathbf{P}^{-\frac{1}{2}}) \mathbf{P}^{\frac{1}{2}}. \quad (14)$$

where $\exp(\mathbf{P})$ is the matrix exponential. The Logarithm map from \mathcal{P}_d to $\mathcal{T}_P\mathcal{P}_d$ is given explicitly by

$$\mathbf{A}_i = \text{Log}_P(\mathbf{P}_i) = \mathbf{P}^{\frac{1}{2}} \log(\mathbf{P}^{-\frac{1}{2}} \mathbf{P}_i \mathbf{P}^{-\frac{1}{2}}) \mathbf{P}^{\frac{1}{2}}. \quad (15)$$

The geodesic metric can be efficiently computed by

$$d_R^2(\mathbf{P}, \mathbf{Q}) = \sum_{i=1}^d \log^2(\lambda_i(\mathbf{Q}^{-1}\mathbf{P}))$$

where $\lambda_i(\mathbf{Q}^{-1}\mathbf{P})$ is the i th eigenvalue of $\mathbf{Q}^{-1}\mathbf{P}$, or the i th general eigenvalue of the pair (\mathbf{P}, \mathbf{Q}) .

The Riemannian mean $\bar{\mathbf{P}}$ of a set $\{\mathbf{P}_i | \mathbf{P}_i \in \mathcal{P}_d\}$ is defined using the Fréchet mean:

$$\bar{\mathbf{P}} = \arg \min_{\mathbf{P} \in \mathcal{P}_d} \sum_i d_R^2(\mathbf{P}, \mathbf{P}_i). \quad (16)$$

The optimization problem (16) is strictly convex and thus, it is well defined, see Bhatia (2009), and can be solved by an iterative procedure. Algorithm 2 computes the *weighted* Riemannian mean. Given a set $\{\mathbf{P}_i \in \mathcal{P}_d\}$ and its mean $\bar{\mathbf{P}}$, a commonly-used Euclidean approximation of the Riemannian distances on \mathcal{P}_d in the neighborhood of $\bar{\mathbf{P}}$ is given by

$$d_R^2(\mathbf{P}_i, \mathbf{P}_j) \approx \|\tilde{\mathbf{A}}_i - \tilde{\mathbf{A}}_j\|_F^2, \quad (17)$$

where $\tilde{\mathbf{A}}_i = \bar{\mathbf{P}}^{-\frac{1}{2}} \text{Log}_{\bar{\mathbf{P}}}(\mathbf{P}_i) \bar{\mathbf{P}}^{-\frac{1}{2}} = \log(\bar{\mathbf{P}}^{-\frac{1}{2}} \mathbf{P}_i \bar{\mathbf{P}}^{-\frac{1}{2}})$ and $\tilde{\mathbf{A}}_j$ is defined analogously. For more details on the accuracy of this approximation, see Tuzel et al. (2008).

Algorithm 2 Weighted Riemannian mean

Input: a set of SPD matrices $\{\mathbf{P}_i\}_{i=1}^N$ and non-negative weights $\{w_i\}_{i=1}^N$ such that $\sum_i w_i = 1$.

Output: the weighted Riemannian mean $\bar{\mathbf{P}}$ satisfying $\bar{\mathbf{P}} = \arg \min_{\mathbf{P} \in \mathcal{P}_d} \sum_i w_i d_R^2(\mathbf{P}, \mathbf{P}_i)$.

- 1: **set:** $\bar{\mathbf{P}} \leftarrow \frac{1}{N} \sum_{i=1}^N w_i \mathbf{P}_i$. {starting point}
 - 2: **do:**
 - 3: **update:** $\bar{\mathbf{S}} \leftarrow \frac{1}{N} \sum_{i=1}^N w_i \text{Log}_{\bar{\mathbf{P}}}(\mathbf{P}_i)$. {weighted Euclidean mean in $\mathcal{T}_{\bar{\mathbf{P}}}\mathcal{P}_d$, see (15)}
 - 4: **update:** $\bar{\mathbf{P}} \leftarrow \text{Exp}_{\bar{\mathbf{P}}}(\bar{\mathbf{S}})$. {see (14)}
 - 5: **while** $\|\bar{\mathbf{S}}\|_F > \epsilon$ { $\|\cdot\|_F$ is the Frobenius norm}
-

7. Regularized Optimal Transport Algorithms

In Algorithm 1 in the paper, Step 4 solves the OT problem. In this section, we describe two possible fast implementations of a regularized version of the classical OT. The first implementation is completely unsupervised, whereas, the second implementation supports a supervised configuration, where the labels of the source set are known.

7.1. Classical Optimal Transport

Given two discrete density vectors, source $\mathbf{c} \in \mathbb{R}^{N_1}$ and target $\mathbf{r} \in \mathbb{R}^{N_2}$, as well as the cost matrix $\mathbf{C} \in \mathbb{R}^{N_1 \times N_2}$, the discrete version of optimal transport is the following optimization problem:

$$\arg \min_{\mathbf{\Gamma}} \langle \mathbf{\Gamma}, \mathbf{C} \rangle \quad (18)$$

such that $\mathbf{\Gamma} \mathbf{1} = \mathbf{c}$ and $\mathbf{\Gamma}^T \mathbf{1} = \mathbf{r}$, where $\mathbf{1}$ is a vector of all ones in a suitable dimension.

7.2. Sinkhorn Optimal Transport

Often, the computation cost of (18) becomes extremely high when the dimensions N_1 and N_2 exceed several hundreds. Cuturi (2013) proposed to solve the optimal transport problem with a regularization term based on entropy, which can be computed with the Sinkhorn's matrix scaling algorithm at a speed that is several orders of magnitude faster than that of classical optimal transport solvers. The proposed regularized problem is:

$$\arg \min_{\mathbf{\Gamma}} \langle \mathbf{\Gamma}, \mathbf{C} \rangle - \frac{1}{\lambda} h(\mathbf{\Gamma}) \quad (19)$$

where $h(\mathbf{\Gamma}) = -\sum_{i=1}^{N_1} \sum_{j=1}^{N_2} \mathbf{\Gamma}[i, j] \log(\mathbf{\Gamma}[i, j])$ is the entropy of $\mathbf{\Gamma}$. We note that in the toy problem in Section 4.1 we assign large values to λ , so that the regularized problem (19) is similar to the classical problem (18). For the real data sets in Section 4.2 and Section 4.3, we set λ adaptively by

$$\lambda = \frac{1}{2m^2}$$

where $m = 0.05 \cdot \text{median} \{ \mathbf{C}[i, j] \}_{i, j}$. We implemented Algorithm 3, which was proposed by Cuturi (2013) and solves (19), as outlined below.

Algorithm 3 Sinkhorn optimal transport proposed by (Cuturi, 2013)

Input: $\mathbf{C} \in \mathbb{R}^{N_1 \times N_2}$, $\lambda \in \mathbb{R}$, $\mathbf{c} \in \mathbb{R}^{N_1}$, and $\mathbf{r} \in \mathbb{R}^{N_2}$.

Output: the transport plan $\mathbf{\Gamma} \in \mathbb{R}^{N_1 \times N_2}$ (solution of (19)).

- 1: **set:** $\mathbf{K}[i, j] \leftarrow \exp(-\lambda \mathbf{C}[i, j])$ $\{\forall i \in \{1, \dots, N_1\} \text{ and } \forall j \in \{1, \dots, N_2\}\}$
 - 2: **set:** $\mathbf{u}[i] \leftarrow \frac{1}{N_1}$. $\{\forall i \in \{1, \dots, N_1\}\}$
 - 3: **set:** $\tilde{\mathbf{K}}[i, j] \leftarrow \frac{\mathbf{K}[i, j]}{\mathbf{c}[i]}$. $\{\forall i \in \{1, \dots, N_1\} \text{ and } \forall j \in \{1, \dots, N_2\}\}$
 - 4: **while** u changes **do:**
 - 5: $\mathbf{z}[j] \leftarrow \frac{\mathbf{r}[j]}{(\mathbf{K}^T \mathbf{u})[j]}$ $\{\forall j \in \{1, \dots, N_2\}\}$
 - 6: **update:** $\mathbf{u}[i] = \frac{1}{(\tilde{\mathbf{K}} \mathbf{z})[i]}$ $\{\forall i \in \{1, \dots, N_1\}\}$
 - 7: **end while**
 - 8: **set:** $\mathbf{v}[j] \leftarrow \frac{\mathbf{r}[j]}{(\mathbf{K}^T \mathbf{u})[j]}$ $\{\forall j \in \{1, \dots, N_2\}\}$
 - 9: **set:** $\mathbf{\Gamma} \leftarrow \text{diag}(\mathbf{u}) \mathbf{K} \text{diag}(\mathbf{v})$
-

7.3. Sinkhorn Optimal Transport with Labels

Consider now a supervised setting consisting of two sets of SPD matrices in \mathcal{P}_d . The source set $\{\mathbf{P}_i, y_i\}_{i=1}^{N_1}$ is given with labels $y_i \in \mathcal{Y}$, where \mathcal{Y} is the set of all possible labels, and the target set $\{\mathbf{Q}_i\}_{i=1}^{N_2}$ is unlabeled (i.e., the labels are unknown). We set $\mathbf{C}_0[i, j] = d_R^2(\mathbf{P}_i, \mathbf{Q}_j)$. Courty et al. (2014) presented a modification of the Sinkhorn optimal transport problem with an additional label regularization term and derived a new efficient algorithm to solve the following problem:

$$\arg \min_{\mathbf{\Gamma}} \langle \mathbf{\Gamma}, \mathbf{C}_0 \rangle - \frac{1}{\lambda} h(\mathbf{\Gamma}) + \eta \sum_{j=1}^{N_2} \sum_{y=1}^{|\mathcal{Y}|} \|\mathbf{\Gamma}(\mathcal{I}_y, j)\|_q^p \quad (20)$$

where \mathcal{I}_y is a set containing the indices of the source points associated with the label $y \in \mathcal{Y}$, $\mathbf{\Gamma}(\mathcal{I}_y, j)$ is a vector consisting of entries from the j th column of $\mathbf{\Gamma}$ associated with the label y (i.e., from rows \mathcal{I}_y) and $\|\cdot\|_q^p$ is the ℓ_q norm to the power of p . See (Courty et al., 2014) for more details. We implemented Algorithm 4, which was proposed by (Courty et al., 2014) and solves (20), as outlined below.

Algorithm 4 Sinkhorn optimal transport with labels proposed by (Courty et al., 2014)

Input: $C_0 \in \mathbb{R}^{N_1 \times N_2}$, $\lambda \in \mathbb{R}$, $\mathbf{c} \in \mathbb{R}^{N_1}$, $\mathbf{r} \in \mathbb{R}^{N_2}$, and the source labels $\{y_i\}_{i=1}^{N_1}$.

Output: the transport plan Γ (solution of (20)).

- 1: **initialize:** $\mathbf{G} \leftarrow \mathbf{0}$ { $\mathbf{G} \in \mathbb{R}^{N_1 \times N_2}$ }
- 2: **do**
- 3: **update** $\mathbf{C} \leftarrow \mathbf{C}_0 + \mathbf{G}$
- 4: **update** $\Gamma \leftarrow \text{SinkhornOptimalTransport}(\mathbf{C}, \lambda, \mathbf{c}, \mathbf{r})$ {Algorithm 3}
- 5: **update** \mathbf{G} according to { $\forall y$ and $\forall j$ }

$$\mathbf{G}(\mathcal{I}_y, j) \leftarrow p \cdot (\|\Gamma(\mathcal{I}_y, j)\| + \epsilon)^{p-1}$$

- 6: **while** Γ changes
-

8. Additional Results

8.1. Application: Illustration on Simulated Data

In the following, we assume that the two sets of SPD matrices $\{\mathbf{P}_i \in \mathcal{P}_d\}_{i=1}^N$ and $\{\mathbf{Q}_i \in \mathcal{P}_d\}_{i=1}^N$ are covariance matrices originating from the raw data sets $\{\mathbf{X}_i \in \mathbb{R}^{d \times M}\}_{i=1}^N$ and $\{\mathbf{Z}_i \in \mathbb{R}^{d \times M}\}_{i=1}^N$. That is, $\mathbf{Z}_i = s(\mathbf{X}_i)$, $\mathbf{P}_i = \text{cov}(\mathbf{X}_i) = \frac{1}{M-1} \mathbf{X}_i \mathbf{X}_i^T$ (assuming zero mean), and $\mathbf{Q}_i = \text{cov}(\mathbf{Z}_i) = \text{cov}(s(\mathbf{X}_i))$ where here s is the mapping between the raw data in the Euclidean space. Alternately, one can replace the $\text{cov}(\cdot)$ function with some other SPD kernel.

In general, under this setting, there are three natural alternatives for applying OT and obtaining the transport plan for domain adaptation. First, applying OT to the raw data with the Euclidean distance as the cost. Second, applying OT to the covariance matrices with the Euclidean distance. Third, applying OT to the covariance matrices with the Riemannian distance d_R . We postulate that the first two methods ignore the geometry of the data sets leading to subpar performance. Conversely, by considering OT with the Riemannian distance d_R on \mathcal{P}_d , we incorporate the geometric structure.

To emphasize this claim, consider the following $N = 40$ time series pairs $(\mathbf{x}^{(i)}(t), \mathbf{z}^{(i)}(t))$:

$$\mathbf{x}^{(i)}(t) = \begin{bmatrix} x_1^{(i)}(t) \\ \vdots \\ x_5^{(i)}(t) \end{bmatrix}, \mathbf{z}^{(i)}(t) = \begin{bmatrix} z_1^{(i)}(t) \\ \vdots \\ z_5^{(i)}(t) \end{bmatrix}, i \in \{1, 2, \dots, 40\}$$

where, for each time stamp t_0 , $\mathbf{x}^{(i)}(t_0), \mathbf{z}^{(i)}(t_0) \in \mathbb{R}^5$ and they are given by

$$\begin{aligned} x_j^{(i)}(t) &= a_j^{(i)} \cos(f_j^{(i)} t + \theta_j^{(i)}) + n_j^{(i)} \\ z_j^{(i)}(t) &= a_j^{(i)} \cos(f_j^{(i)} t + \phi_j^{(i)}) + \eta_j^{(i)}, \quad j \in \{1, 2, \dots, 5\}, \end{aligned}$$

Namely, $x_j^{(i)}$ and $z_j^{(i)}$ are cosine function with the same frequency $f_j^{(i)}$ and the same amplitude $a_j^{(i)}$. The two signals are differ in phase and noise. Specifically, $a_j^{(i)}, f_j^{(i)} \sim U[0, 20]$, $\theta_j^{(i)}, \phi_j^{(i)} \sim U[0, 2\pi]$, and $n_j^{(i)}, \eta_j^{(i)} \sim \mathcal{N}(0, 1)$. We denote

$$\begin{aligned} \mathbf{X}_i &= [\mathbf{x}^{(i)}(0) \quad \mathbf{x}^{(i)}(T_s) \quad \mathbf{x}^{(i)}(2T_s) \quad \dots \quad \mathbf{x}^{(i)}(1)] \in \mathbb{R}^{5 \times T} \\ \mathbf{Z}_i &= [\mathbf{z}^{(i)}(0) \quad \mathbf{z}^{(i)}(T_s) \quad \mathbf{z}^{(i)}(2T_s) \quad \dots \quad \mathbf{z}^{(i)}(1)] \in \mathbb{R}^{5 \times T} \end{aligned}$$

where $T_s = 0.01$ and $T = 101$. Figure 6(a) displays realizations of \mathbf{X}_1 and \mathbf{Z}_1 . Let $\mathbf{P}_i = \text{cov}(\mathbf{X}_i)$ and $\mathbf{Q}_i = \text{cov}(\mathbf{Z}_i)$. Given the two sets $\{\mathbf{X}_i\}_i$ and $\{\mathbf{Z}_i\}_i$, we apply the three configurations of the OT to: (i) the two sets with Euclidean distance, (ii) to their covariance matrices with Euclidean distance and (iii) to their covariance matrices with the Riemannian distance d_R . Figure 6(b-d) presents the obtained transport plan for each configuration. The first configuration (raw data), Fig. 6(b), is sensitive to time shifts and thus it provides a poor matching. The covariance matrices capture a more global structure, and thus, are less sensitive to time shifts. Hence, the second configuration (covariances with Euclidean distance) in Fig. 6(c) performs better than the first configuration, but not as good as the last configuration (covariances with Riemannian distance) in Fig. 6(d), which provides a near perfect matching.

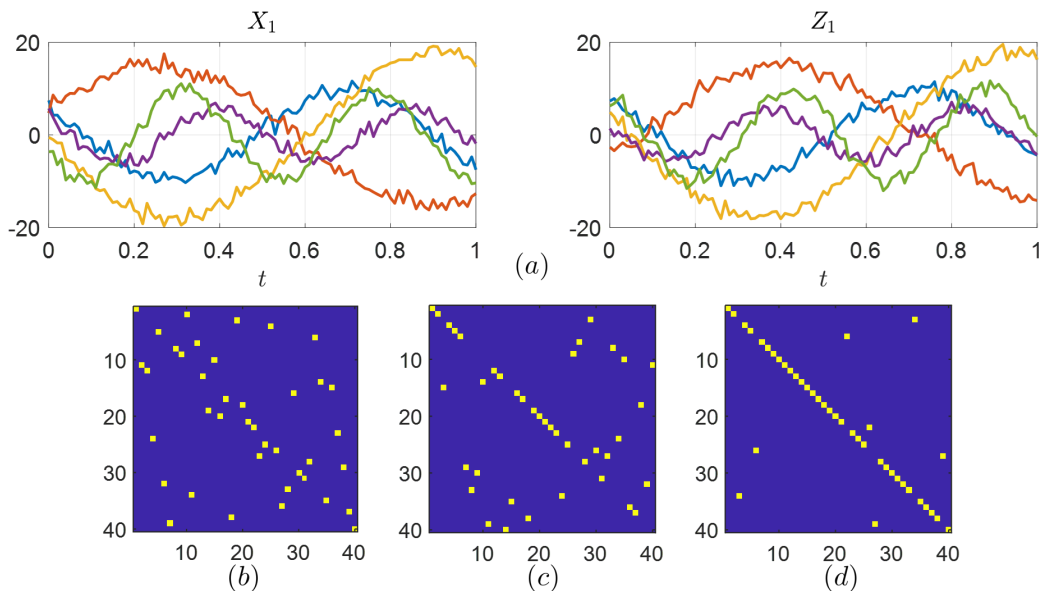


Figure 6. (a) Realizations of X_1 and Z_1 . Bottom, the transport plans obtained by OT applied to: (b) The two sets $\{X_i\}_i$ and $\{Z_i\}_i$ with Euclidean distance. (c) The covariance matrices $\{P_i\}_i$ and $\{Q_i\}_i$ with Euclidean distance. (d) The covariance matrices $\{P_i\}_i$ and $\{Q_i\}_i$ with the Riemannian distance d_R .

Therefore, as demonstrate in the main paper (see Section 4), the Riemannian distance facilitates meaningful comparisons and enables us to achieve state of the art performance in applications.

8.2. Motor imagery task

Prior to computing the covariance matrices, we applied a band pass filter with cutoff frequencies 8Hz and 30Hz (see the ‘GetEvents.m’ script for the implementation). This preprocessing was performed in the previous works (Barachant et al., 2012; Zanini et al., 2018; Yair et al., 2019), where this data set was used.

In the main paper, we provide an illustrative result to the cross-session adaptation. We now test the adaptation of five sets corresponding to all subjects². One set corresponding to Subject 1 was set as the reference set. Then, we applied Algorithm 1 to the remaining sets of the 4 subjects, mapping them one by one to the reference set. Figure 7(a) displays the 2-dimensional t-SNE representation to the SPD matrices of all five subjects (in session 1). Figure 7(b) displays the 2-dimensional t-SNE representation of the SPD matrices after applying Algorithm 1 (unsupervised). Figure 7(c) displays the 2-dimensional t-SNE representation of the SPD matrices after applying Algorithm 1 (supervised). We observe that after the adaptation the SPD matrices are clustered by label of the trial and not by subject. In addition, similarly to the experiments in the main paper, we clearly observe the contribution of the labels in the supervised setting.

Finally, Table 3 provides the cross-subject classification accuracy, extending Table 1(b), which appears in Section 4.2. The left part of the table displays the pairwise classification accuracy when one subject used a train set and another a test set. We observe that overall Algorithm 1, with the Riemannian metric, provides the best results

8.3. Event related potential P300 task

Prior to computing the covariance matrices, we applied a band pass filter with cutoff frequencies 1Hz and 24Hz. This preprocessing is implemented in the py.BI.EEG.2013-GIPSA github code. A similar preprocessing was also applied in (Barachant & Congedo, 2014). We denote the data from i th trial of the k th subject by $X_i^{(k)} \in \mathbb{R}^{16 \times 512}$. Note that the empirical covariance matrix is invariant to the temporal order of the samples, yet the ERP is a short local wave. Consequently, the covariance matrix does not capture sufficient information on the ERP in a given trial. Thus, instead of the standard covariance matrix, we use an augmented covariance matrix as proposed by Barachant & Congedo (2014) by concatenating

²As reported in the paper, we consider only 5 subject out of the available 9. See the explanation in Section 4.2 for details.

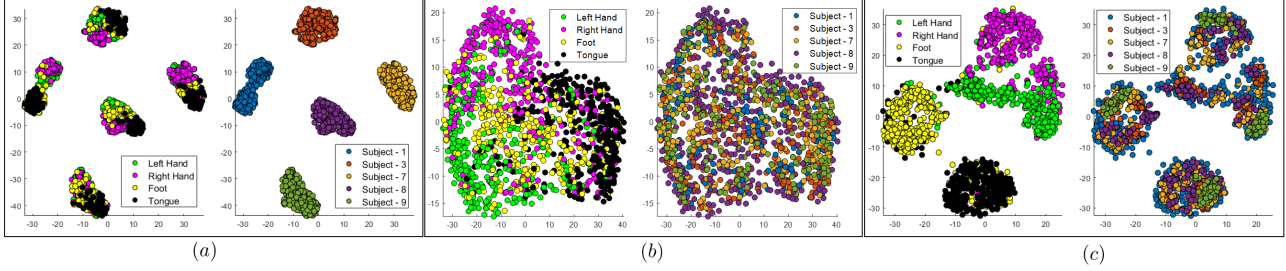


Figure 7. Multi-subject domain adaptation of the data from the BCI motor imagery task. (a) 2-dimensional t-SNE representation of all the SPD matrices of all five subjects (in Session 1). (b) 2-dimensional t-SNE representation after applying Algorithm 1 (unsupervised). (c) 2-dimensional t-SNE representation after applying Algorithm 1 (supervised).

Table 3. Cross-subject classification accuracy in the motor imagery task. The four right-most columns consist of the mean results obtained per subject. Alg. 1 stands for Algorithm 1, Alg. 1 (Euclid) stands for Algorithm 1 when the Euclidean distance is used instead of the Riemannian distance d_R . PT stands for domain adaptation using Parallel Transport by Yair et al. (2019). AT stands for the domain adaptation using Affine Transform by Zanini et al. (2018). The ± 7 is the overall standard deviation of Algorithm 1.

Test sub.	Train sub.					Alg. 1	Alg. 1 (Euclid)	PT	AT
	1	3	7	8	9				
1		78.13	67.36	70.14	55.90	67.88	61.98	60.31	60.4
3	78.13		79.17	78.13	66.67	75.52	70.40	65.02	69.4
7	63.54	70.49		62.50	68.40	64.76	60.85	57.03	57.0
8	68.06	72.22	67.01		66.32	68.92	65.97	59.81	63.2
9	52.43	67.36	72.22	75.00		66.75	56.43	63.63	68.8
Mean						68.92 ± 7	63.13	61.16	63.76

artificial channels to the data. While Zanini et al. (2018) used the true hidden labels for that purpose, we apply a practical approach in unsupervised settings which does not require access to the hidden labels. In (Zanini et al., 2018), the augmented covariance matrices were computed as follows. Let $\mathcal{T}^{(k)}$ be the trials of the k th subject containing an ERP response. The knowledge of $\mathcal{T}^{(k)}$ is unavailable since this set contains the labels we try to classify. If $\mathcal{T}^{(k)}$ were given, the average ERP response can be computed by:

$$\bar{\mathbf{X}}^{(k)} = \frac{1}{|\mathcal{T}^{(k)}|} \sum_{i \in \mathcal{T}^{(k)}} \mathbf{X}_i^{(k)} \in \mathbb{R}^{16 \times 512}.$$

Next, the average response $\bar{\mathbf{X}}^{(k)}$ is appended to the data of each trial, obtaining:

$$\tilde{\mathbf{X}}_i^{(k)} = \begin{bmatrix} \bar{\mathbf{X}}^{(k)} \\ \mathbf{X}_i^{(k)} \end{bmatrix} \in \mathbb{R}^{32 \times 512}.$$

Then, the augmented empirical covariance of $\tilde{\mathbf{X}}_i^{(k)}$, denoted by $\tilde{\mathbf{P}}_i^{(k)} \in \mathbb{R}^{32 \times 32}$, is computed.

Here, we propose a different approach, which does not require the knowledge of $\mathcal{T}^{(k)}$. For each subject k , we apply the ERP detector proposed by Hoffmann et al. (2005) to all 480 trials. The overall accuracy of this ERP detector was very low and it cannot be used as a stand-alone method for classification of data from multiple subjects. However, when considering only the 15 trials for each subject k with the highest confidence score provided by the detector as trials with an ERP response, we approximate a subset of $\mathcal{T}^{(k)}$. In turn, this subset is used to compute the augmented covariance matrices similarly to the procedure described above. We remark that on average 12 out of the 15 trials indeed include an ERP response.

It is important to note that the entire data set contains 24 subjects. We test our algorithm on 6 six subjects discussed in (Zanini et al., 2018) (4 “good” subjects and 2 “bad” ones), and we use the remaining subjects to train the P300 detector. Consequently, the P300 detector and the proposed domain adaptation algorithm do not share the same data.

Table 4. Classification precision of Algorithm 1 (unsupervised) in the ERP P300 task

Test sub. \ Train sub.	1	2	3	4	5	6	Mean
1		88.06	91.30	88	90.62	86.30	88.85
2	90.90		92.53	88.57	86.11	85.29	88.68
3	97.10	97.22		97.33	93.15	94.66	95.89
4	94.91	95.08	95.08		88.23	96.66	93.99
5	97.22	97.22	86.30	97.29		94.66	94.54
6	94.91	94.66	91.30	92.53	76.60		90.00
Mean	95.01	94.45	91.30	92.74	86.94	91.51	91.99±3.9

Table 5. Classification precision of Algorithm 1 (supervised) in the ERP P300 task

Test sub. \ Train sub.	1	2	3	4	5	6	Mean
1		93.94	93.94	90.91	92.68	86.36	91.57
2	96.77		90.91	91.43	93.94	75.51	89.71
3	97.73	97.87		95.56	95.56	95.35	96.05
4	97.06	100	100		95.83	97.44	98.07
5	98.21	96.49	93.94	98.36		93.33	96.07
6	88.37	85.71	76.60	84.00	92.50		85.44
Mean	95.62	94.80	91.07	92.05	94.10	89.59	92.87±6.1

Finally, Table 4 provides the cross-subject classification accuracy, extending the unsupervised column in Table 2, which appears in Section 4.3. Similarly, Table 5 extends the supervised column in Table 2 as well. We observe that Algorithm 1 provides the best results overall, and that the knowledge of the labels in the supervised setting improves the classification.

9. Source code

Our Matlab source code is available in the attached ZIP file. Please notice that in order to apply the code to the data sets, they need to be downloaded first from the following links.

9.1. Toy problem

For the toy examples we use [this](#) OT solver (we include this package in our SM.zip file). The toy example can be fully run using the two scripts in the ToyExample folder.

- The script ‘MainPlotCone.m’ generates figures (a) and (b) in Figure 2 in the paper.
- The script ‘MainPlotPlan.m’ generates figures (c) and (d) in Figure 2 in the paper.

9.2. Motor imagery task

- The data is available [here](#) (data set 2a) and described [here](#).
- We read the data files using [BioSig](#).
- The ‘GetEvents.m’ script (function) reads the data and applies a simple preprocessing to it as reported in the previous works by Barachant et al. (2012); Zanini et al. (2018); Yair et al. (2019).
- The ‘MainBciPlot.m’ script applies the proposed algorithm for domain adaptation to the data. The script plots the t-SNE representation before and after the adaptation similarly to the figures in the paper and trains a classifier accordingly.

9.3. Event related potential P300 task

- The data is available [here](#) and described [here](#).

Optimal Transport on the Manifold of SPD Matrices for Domain Adaptation

- We used the [py.BI.EEG.2013-GIPSA](#) repository to read the data files and to save them in '.mat' format.
- The 'MainErpPlot.m' script applies the proposed algorithm for domain adaptation to the data. The script plots the t-SNE representation before and after the adaptation similarly to the figures in the paper and trains a classifier accordingly.
- For computing the appended covariance features, we used this [this](#) P300 detector. One can download it and replace line 23 in the script.